Comparative Study of Liquid−Solid Phase Transition of Nitrogen in Controlled Pore Glass and SBA-15: Accurate Pore Size of Conventional Mesoporous Materials

Kunimitsu Morishige,* Hiroaki Uematsu, and Noriko Tateishi

Department of Chemistry, Okayama University of Science, 1-1 Ridai-cho, Okayama 700-0005, Japan

Received: May 30, 2003; In Final Form: February 4, 2004

To elucidate the origin of the discrepancies in pore size dependences of the melting temperature of the confined solids and the hysteresis temperature of the gas−liquid-phase transitions between conventional mesoporous materials and mesoporous molecular sieves, we performed measurements of the adsorption−desorption isotherm over a wide temperature range for N_2 confined in the interconnected pores of controlled pore glass with a nominal pore diameter of 11.5 nm and the cylindrical pores of SBA-15 with a mean pore diameter of 9.4 nm, as well as the X-ray diffraction pattern as a function of temperature. A hysteresis loop in the adsorption−desorption isotherm shrank with increasing temperature and eventually disappeared at a hysteresis temperature well below the bulk critical point. On the other hand, when the temperature was decreased well below the bulk triple point, the adsorption hysteresis still survived. The inflection points in the $\Delta\mu-T$ curve of capillary condensation and evaporation were nearly consistent with the freezing and melting temperatures determined by X-ray diffraction, respectively. The shifts of these characteristic temperatures relative to the bulk values for controlled pore glass were considerably smaller than those for SBA-15, although the nominal pore size of controlled pore glass was not very different from the pore size of SBA-15. All these results confirm the discrepancies in characteristic temperature shifts between the conventional mesoporous materials and the mesoporous molecular sieves inferred from a comparison of the literature data for the two types of adsorbents. The coherence length of the solid N_2 formed inside the interconnected pores of controlled pore glass was significantly larger than the nominal pore diameter, whereas that of the solid N_2 inside the cylindrical pores of SBA-15 was only slightly larger than the mean pore diameter. This strongly suggests that the pore sizes of controlled pore glass and other conventional mesoporous adsorbents are actually greater than specified.

I. Introduction

When a mesoporous solid is exposed to a vapor, capillary condensation occurs at a gas pressure smaller than the pressure of the saturated vapor at a given temperature. Experimentally, capillary condensation is characterized by a distinct step in an adsorption isotherm often accompanied by a hysteresis loop.[1] The hysteresis loop shrinks with increasing temperature and eventually disappears at a hysteresis temperature (T_h),[2] which depends on the mean pore size but lies below the critical temperature (T_c) of the bulk fluid. T_h is not necessarily equal to a so-called pore critical temperature (T_{cp}) at which a gas−liquid coexistence in pores vanishes,[3−6] although the determination method and nature of T_{cp} are not yet confirmed. When the temperature is decreased well below the bulk triple point (T_t), a capillary condensate is expected to solidify. These gas−liquid and liquid−solid phase transitions in confinement have attracted a great deal of attention in recent years.[7]

Two types of mesoporous materials, conventional mesoporous solids and mesoporous molecular sieves, are widely used in the experiments. The conventional mesoporous materials such as porous glass and silica gel consist of an interconnected network of pores of varying shape, curvature, and size.[7,8] On the other hand, the main pores of MCM-41[9] and SBA-15[10] mesoporous molecular sieves are cylindrical and their pore size distributions are sharp compared to those of the conventional mesoporous adsorbents. Recently, we have examined the phase transitions of several gases and liquids confined to the cylindrical pores of the mesoporous molecular sieves. During the course of these studies we found out that the pore-size dependences of the hysteresis temperature and liquid−solid phase transition temperature of confined phases for the mesoporous molecular sieves would be significantly larger than those for the conventional mesoporous materials. For example, CO_2 and Xe on Vycor glass,[2] Ar and Xe on Silicagel,[11] and N_2, Xe, and SF_6 on controlled pore glass[12] show significantly smaller shifts of T_h than on MCM-41[4,13] and SBA-15.[14] The melting point depressions of ice in controlled pore glass[15] are considerably smaller than those in MCM-41[16,17] and SBA-15.[17] Although these discrepancies occasionally have been ascribed to a pore networking effect[7,18] or inaccuracy[17] of nominal pore size of the conventional mesoporous materials, their origin remains obscure.

Nitrogen is a standard gas for exploring the porous structure of materials by a gas adsorption method.[1] The critical point of the gas−liquid coexistence is 126.2 K. Liquid nitrogen solidifies at a low temperature. The β phase of nitrogen, which is hcp with a practically ideal c/a ratio, exists between 35.6 nd 63.1 K.[19,20] The molecules are orientationally disordered due to rapid reorientations. The liquid−solid transitions of nitrogen confined in porous glass[21,22] and MCM-41 mesoporous molecular sieve[23] have been investigated by means of X-ray diffraction. Upon cooling, the confined phase solidified in the hcp structure with an appreciable number of stacking faults. When the results on

* Address correspondence to this author. E-mail:morishi@chem.ous.ac.jp.

10.1021/jp030696t CCC: $27.50
Published on Web 05/04/2004

both porous glass and MCM-41 are compared, however, it is also inferred that the pore-size dependence of the phase transition temperatures for MCM-41 is significantly larger than that for porous glass. The purpose of the present study is to elucidate the origin of the discrepancies between the results obtained on both types of adsorbents. First, we examined the temperature dependence of the adsorption−desorption isotherm of nitrogen onto controlled pore glass with a nominal pore diameter of 11.5 nm and SBA-15 with a mean pore diameter of 9.4 nm over a wide temperature range between $<T_t$ and T_c, to obtain freezing (T_f) and melting (T_m) temperatures, as well as T_h and T_{cp}, of nitrogen in both types of adsorbents and confirm the above-mentioned discrepancies. Next, we examined the liquid−solid phase transitions of the nitrogen confined to the interconnected pores of controlled pore glass and the cylindrical pores of SBA-15 by means of X-ray diffraction. This gives direct determinations of T_f and T_m. In addition, we are able to obtain a crystallite size of solid nitrogen inside the pores from the diffraction line broadening. Finally, the origin of the discrepancies will be discussed on the basis of these results.

II. Experimental Section

Controlled pore glass (CPG00120A) was supplied by CPG Inc., USA. It is produced from a borosilicate bare material that is heated to separate the borates and the silicates. The borates are leached out from the material, leaving the silica glass with controlled but interconnected pores of irregular shape. According to the manufacturer, its mean pore diameter (the mercury intrusion method) is 11.5 nm with a pore size distribution of 7.3%. The specific pore volume and surface area are 0.49 cm^3/g and 119.5 m^2/g, respectively. SBA-15 was prepared by using Pluronic 123 triblock copolymer at an aging temperature of 373 K according to the procedure of Kruk et al.[24] The as-synthesized material was calcined for 4 h at 823 K in a flow of air. The resulting material showed a well-resolved hexagonal XRD pattern. The mean pore diameter (D) of 9.4 nm was obtained from comparing the adsorption branch of nitrogen at 77 K with the equilibrium pressures[25] calculated on the basis of nonlocal density functional theory (NLDFT) for the cylindrical pores of siliceous mesoporous materials.

Adsorption isotherms were measured volumetrically on two types of homemade semiautomated instruments equipped with manometers of full scales of 100 and 25 000 Torr, respectively. The experimental apparatus and procedures have been described in detail elsewhere.[13,14] Calculation of adsorption at higher pressures took gas nonideality into consideration on the basis of a modified BWR equation.[26] The temperatures were regulated within ±0.05 K with a temperature controller (Scientific instruments, type 9650) having a Si diode temperature sensor.

The experimental apparatus of X-ray diffraction for freezing/melting measurements also has been described in detail elsewhere.[27] The measurements were carried out with Cu Kα radiation in a Bragg−Brentano geometry. About 0.2 g of CPG and SBA-15 were packed in a sample holder of Cu, covered with a 0.1 mm thick sheet of Be, and then attached to a cold head of a He closed-cycle refrigerator. After prolonged evacuation at room temperature, the substrate was cooled and then the background spectrum was measured. An adsorption isotherm of nitrogen inside the X-ray cryostat was measured at 67 K. The substrate was then cooled to a desired temperature between 67 and 32 K, and the spectrum was measured. The diffraction pattern of the confined phase was obtained by subtraction of data for charged and empty substrates.

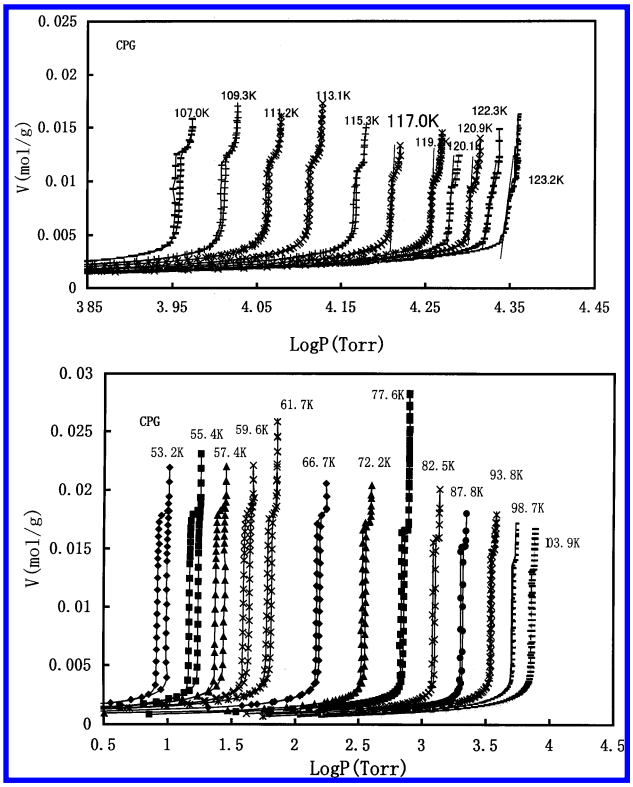

Figure 1. Temperature dependence of the adsorption−desorption isotherm of N_2 onto CPG over a wide temperature range of 53−123 K.

III. Results and Discussion

III. 1. Isotherms. The adsorption isotherms of simple gases onto disordered mesoporous solids at low temperatures usually exhibit large hysteresis loops of type H2 in the IUPAC classification.[28] In this type of hysteresis, the slope of the adsorption step has a finite value. This gives some doubt as to the occurrence of capillary condensation in disordered mesoporous solids and makes elusive the relation between T_h and T_{cp}, because one cannot identify T_{cp} with the disappearance of a vertical jump in the adsorption isotherm or the sudden change in slope of the adsorption step. However, the present CPG sample gives a hysteresis loop of type H1, in contrast to most of the conventional mesoporous materials. Figure 1 shows the adsorption−desorption isotherm of N_2 onto the CPG of a nominal pore diameter of 11.5 nm as a function of temperature. At low temperatures, the adsorption and desorption branches are parallel to each other and also almost parallel to a bulk condensation line. This proves that capillary condensation of a first-order transition actually occurs within the interconnected pores of this sample. We estimated the specific surface area and total pore volume to be 116 m^2/g and 0.51 cm^3/g, respectively, from the BET monolayer capacity and saturated amount of adsorption at 77.6 K, being in reasonable agreement with the manufacturer's data. The porosity of the CPG was estimated to be 0.53 from the density of bulk silica (2.2 g/cm^3) and the pore volume. When the temperature was increased, the hysteresis loop shrank and eventually disappeared at 117 K. The adsorption steps were still vertical above 117 K. This indicates that T_h is lower than T_{cp}, in accord with the results on the mesoporous molecular sieves with unconnected cylindrical pores.[4,6,14] T_{cp} locates around 122 K, because the slope of the adsorption step begins to decrease at 122.3 K. Such a change of a vertical to steep step on crossing a critical point has been

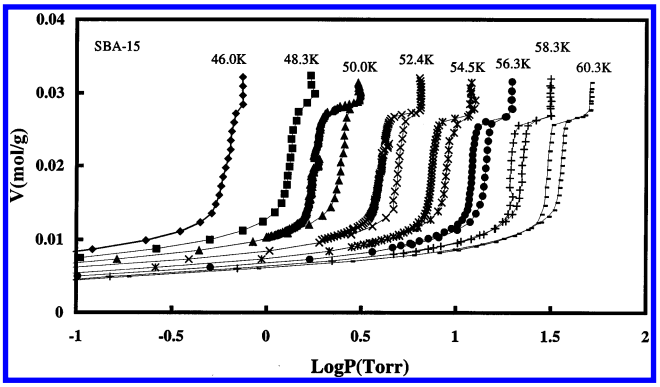

Figure 2. Temperature dependence of the adsorption−desorption isotherm of N_2 onto SBA-15 in the temperature range of 46−60 K. Only adsorption isotherms were measured at 46.0 and 48.3 K.

also observed for ^{4}He confined in silica aerogel with a high porosity and exceedingly wider pores.[29]

The relation between the adsorption−desorption isotherm and the liquid−solid phase transitions of a confined phase has been a matter of some controversy in the past several decades. Litvan and McIntosh[30] and Burgess et al.[2] have reported that the hysteresis loop shrinks with decreasing temperature and eventually disappears well below T_t. On the other hand, Huber and Knorr[31] have revealed from very careful experiments that the disappearance of the hysteresis loop well below T_t often observed comes from an intermediate unstable state occurring in the final part of the adsorption branch and the adsorption hysteresis survives still in the solid state. They related the inflection points in the chemical potential (μ)−temperature curve of capillary condensation (adsorption) and evaporation (desorption), respectively, to the solidification in a quasiisosteric cooling scan and the melting in a quasiisosteric heating scan. It is expected that in pores thermodynamically stable gas−liquid and gas−solid coexistence curves intersect each other at a pore triple point (T_{tp}), similar to a bulk fluid. Duffy and Alam[32] have constructed an adsorption desorption phase diagram for capillary confined CO_2 using positron/positronium annihilation spectroscopy. In their diagram the hysteresis loop decreases in width with decreasing temperature and eventually disappears at T_{tp}, as opposed to the results of Huber and Knorr.[31] All these studies[2,30−32] were performed on conventional mesoporous materials having a three-dimensional network structure of irregular pores. In our previous work,[33] we examined the relationship between the adsorption isotherm and freezing of Kr in SBA-15. Although we were able to confirm partly the results of Huber and Knorr,[31] the poor quality of the SBA-15 substrate used prevented us from elucidating the relationship between the inflection points of the $\mu-T$ curve and the liquid−solid transitions of the confined phase.

When the temperature was decreased well below T_t, the adsorption hysteresis still survived. This is opposed to the results of Litvan and McIntosh,[30] Burgess et al.,[2] and Duffy and Alan,[32] and gives support to the results of Huber and Knorr.[31] Figure 2 shows the temperature dependence of the adsorption−desorption isotherms of N_2 on SBA-15 of $D = 9.4$ nm in the temperature range 46−60 K. When the temperature was decreased well below T_t, the hysteresis still survived similarly to CPG. Figure 3 shows the difference in chemical potential for capillary condensation and evaporation of the N_2 within the interconnected pores of CPG and the cylindrical pores of SBA-15. Here the difference of the chemical potential is expressed as $\Delta\mu = \mu - \mu^{bulk} = RT\ln(P/P_0)$ and the chemical potential of the bulk liquid is used as the origin of the μ scale. This figure also

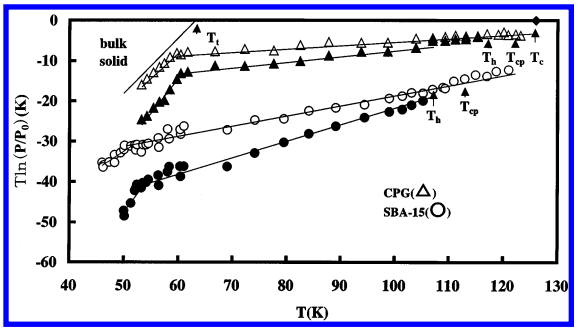

Figure 3. Difference of chemical potential for capillary condensation (open symbols) and evaporation (closed symbols) of the N_2 in CPG and SBA-15 with respect to the bulk liquid.

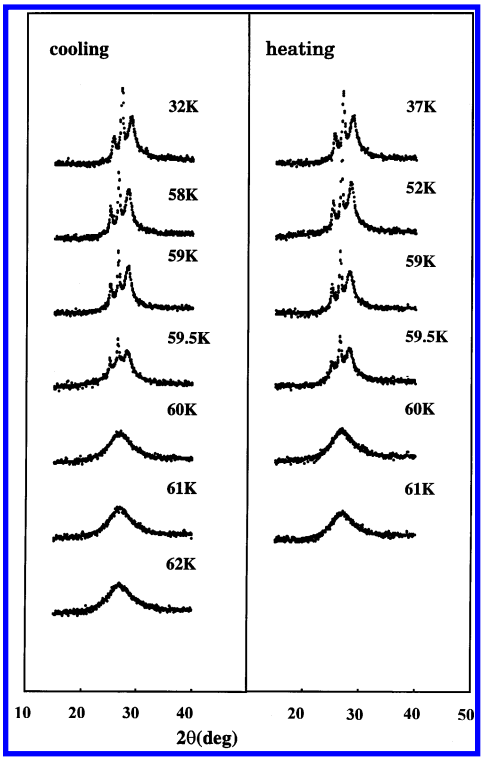

Figure 4. Change of the X-ray diffraction pattern of the N_2 confined to the interconnected pore of CPG upon cooling and heating.

contains the data obtained previously[14] at higher temperatures on SBA-15. T_h and T_{cp} of N_2 in SBA-15 were ∼107 and ∼112 K, respectively. Both the slopes of the $\Delta\mu_a-T$ and $\Delta\mu_d-T$ plots in CPG showed sharp changes around 60 K, strongly suggesting that a thermal hysteresis between solidification and melting is small. The freezing and melting temperatures of N_2 in SBA-15 are inferred to be ∼51 and ∼53 K, respectively, from the inflection points in the $\Delta\mu-T$ curve of capillary condensation and evaporation in SBA-15. The shifts of T_h and T_{cp} relative to T_c and of T_f and T_m relative to T_t for CPG are considerably smaller than those for SBA-15, although the nominal pore diameter of CPG is not very different from the pore diameter of SBA-15. In any event, it is evident that the confined solid is stable compared to the bulk solid, irrespective of porous structures, and capillary sublimation between a gas and a solid takes place in the pores in a process similar to capillary condensation.

III. 2. X-ray Diffraction. Figure 4 shows the diffraction patterns of the confined N_2 for CPG on first cooling and subsequent heating scan through the liquid−solid transitions. On cooling, the diffraction pattern suddenly changed at 59.5 K; the broad peak centered at $2\theta = 27°$ splits into three sharp

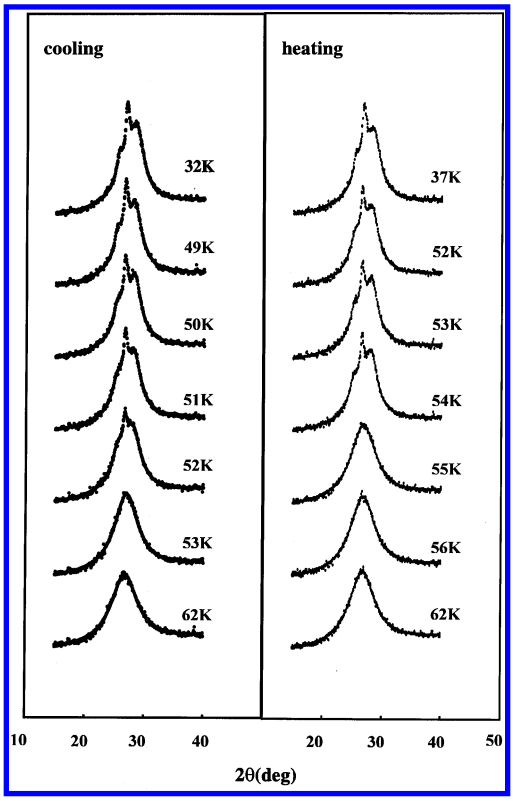

Figure 5. Change of the X-ray diffraction pattern of the N_2 confined to the cylindrical pores of SBA-15 upon cooling and heating.

peaks at $2\theta = 25.0$, 26.5, and 28.2°. This indicates the onset of solidification. These three peaks can be indexed to the (100), (002), and (101) reflections of the hcp β-N_2, respectively. On heating, the solid melted at 60 K. Figure 5 shows the diffraction patterns of the confined N_2 for SBA-15. The liquid−solid phase transitions of N_2 within SBA-15 took place at considerably lower temperatures than those within CPG. The diffraction pattern suddenly changed from a liquid to a solid form at 52 K on cooling and vice versa at 55 K on heating. The positions and relative intensities of the three peaks for SBA-15 were identical to those for CPG within the limits of experimental accuracy, although the peak widths for SBA-15 were considerably larger than those for CPG. This strongly suggests that the structures of the solid N_2 confined to the cylindrical pores of SBA-15 and the interconnected pores of CPG are almost the same and only the crystallite sizes differ from each other. The three peaks shifted to higher scattering angle with decreasing temperature, indicating thermal shrinkage of the microcrystals in the pores. The freezing and melting temperatures determined by X-ray diffraction nearly coincide with the inflection points in the $\Delta\mu - T$ curves of capillary condensation and evaporation, in good agreement with the results of Huber and Knorr.[31] Figure 6 shows the shifts of T_m relative to T_t for N_2 confined in CPG and SBA-15 as a function of inverse pore diameter, as compared to those for porous glass[22] and MCM-41.[23] The data points for CPG and SBA-15 fit the pore-size dependences of T_m for porous glass of Huber et al.[22] and for MCM-41 of Morishige and Kawano,[23] respectively. The melting-point depressions for the mesoporous molecular sieves are significantly larger than those for the conventional mesoporous materials.

Previous studies[21,23] have shown that upon cooling the N_2 confined to the mesopores of porous glass and MCM-41 solidifies in the hcp structure with an appreciable amount of stacking faults. The main peak is composed of the (100), (002), and (101) reflections of the hcp β-N_2. The stacking faults result

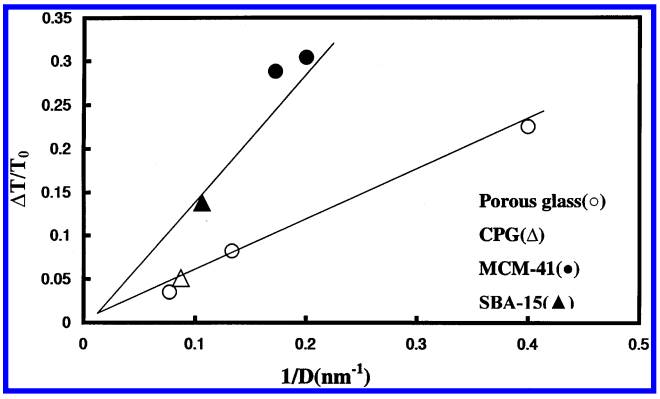

Figure 6. Melting point depressions of the solid N_2 confined to the interconnected pores of the conventional mesoporous materials and the unconnected cylindrical pores of the mesoporous molecular sieves as a function of the inverse pore diameter: Huber et al.[22] (○), Morishige and Kawano[23] (●), and this work (△, ▲). Solid lines are only guides for the eyes.

in broadening of the (100) and (101) reflections. Within the limits of experimental accuracy the X-ray peak broadening for SBA-15 was almost independent of temperature. On the other hand, a slight tendency to broadening of all three main peaks was observed with decreasing temperature for CPG. This suggests that upon cooling competition between molecule−wall and molecule−molecule interactions takes place in the pores of CPG and results in a lowering of long-range order because of the difference in thermal expansivity between pore wall and solid N_2. The coherence length of the microcrystals formed in CPG and SBA-15 was estimated from the width of the (002) reflection by using the Scherrer equation. Taking into account corrections for instrumental broadening, the average sizes of the solid N_2 confined in CPG and SBA-15 can be estimated to be 31 and 12 nm, respectively. The coherence length of the solid N_2 in CPG is significantly larger than the nominal pore diameter of the matrix, whereas that in SBA-15 is only slightly larger than the pore diameter. It is often reported that the coherence length of the solids formed inside the interconnected pores of porous glass are significantly larger than the pore sizes of the matrixes.[22,23,34−37] Such differences in pore sizes and crystallite sizes have been explained by the formation of single crystallites with long-range translational correlations that extend over several different pores[34−36] or by the formation of crystallites which are grown along the pores over quite a distance.[22,23,37] It means that the crystallization front spreads along the pores upon cooling. If this were true, the coherence lengths of the solids formed inside the cylindrical pores of the mesoporous molecular sieves would be considerably larger than the pore sizes as well. As the present results clearly show, however, they are always comparable to the pore diamters.[23,38−40] This fact gives some doubt as to the value of the pore size reported for porous glass and CPG. The differences in pore sizes and crystallite sizes strongly suggest that the pore sizes of porous glass and other conventional porous materials are actually greater than specified. On the other hand, the pore sizes of the mesoporous molecular sieves have been determined on the basis of crystallographic data and thus their absolute values are reliable.

III. 3. Accurate Pore Size of CPG. The adsorption hysteresis of N_2 is often used for calculations of a pore size distribution (PSD) of porous materials,[1] where pore size is determined from the relative pressure of the adsorption−desorption hysteresis. As Figure 3 shows, capillary condensation and evaporation pressures of N_2 for CPG are considerably higher than those for

SBA-15, although the nominal pore size of CPG is not very different from the pore size of SBA-15. This strongly suggests that the real pore size of CPG is considerably larger than that of SBA-15. The pore size of the conventional mesoporous materials should be calculated by using the adsorption branch, because a pore blocking effect occurs for the desorption branch.[41] The condensation pressure depends on the pore size and shape and also on the strength of the interaction between the fluid and pore walls. If we assume that the pores of CPG consist of a collection of independent cylindrical pores such as MCM-41 and SBA-15,[42,43] its mean pore diameter is estimated to be ∼30 nm from comparing the observed adsorption branch of N_2 at 77 K with the NLDFT isotherms[25] for the unconnected cylindrical pores. This value is compatible to the coherence length of the microcrystals of N_2 formed inside the interconnected pores of CPG, although it is surprisingly large compared to the nominal pore diameter of 11.5 nm. If the real pore diameter of CPG was indeed ∼30 nm, the small shift in T_m of the liquid−solid transition, as well as the small shifts in T_h and T_{cp} of the gas−liquid transition, would be well accounted for within the framework of the linear relationship between the inverse pore size and the characteristic temperature shifts established for the unconnected cylindrical pores of the mesoporous molecular sieves. This suggests that the effect of pore-connectivity on phase transition temperatures is insignificant, in good agreement with our previous results on MCM-48 with a well-defined three-dimensional network structure of cylindrical pores.[44]

Porosity data of the present CPG sample were determined by the mercury intrusion method. The PSD of conventional mesoporous materials is most often obtained from the mercury intrusion method or from applying the Barrett−Joyner−Halenda (BJH)[45] method to nitrogen adsorption isotherms at 77 K. In a very recent work,[46] we have shown that in cylindrical pores capillary condensation rather than capillary evaporation takes place near a thermodynamical equilibrium point, although it is opposed to the general statement that capillary evaporation takes place at the equilibrium. The justification relied on the simple idea that the equilibrium phase transition pressures in hysteretic isotherms would be obtained by the extrapolation of the pressure−temperature plot for reversible capillary condensation to lower temperatures. The accurate pore size of conventional mesoporous materials can be evaluated by comparing the experimental adsorption branch with the relationship between pore size and equilibrium capillary condensation pressure reported in the literature including the BJH method under the assumption that the pores are cylindrical. Instead, the use of the experimental desorption branch leads to large underestimation of pore size. The pore sizes thus obtained, of course, depend on the relationship employed. Very recently, Qiao, Schoenhoff, and Findenegg[47] have reported that the pore sizes of two types of CPG are actually larger than specified.

IV. Conclusions

The shifts of T_h and T_{cp} relative to T_c and of T_f and T_m relative to T_t for CPG are considerably smaller than those for SBA-15, although the nominal pore diameter of CPG is not very different from the pore diameter of SBA-15. The coherence length of the solid nitrogen in CPG is significantly larger than the nominal pore diameter of the matrix, whereas that in SBA-15 is only slightly larger than the pore diameter. If we assume that the pores of CPG consist of a collection of independent cylindrical pores such as MCM-41 and SBA-15, its mean pore diameter is estimated to be ∼30 nm from comparing the adsorption branch of N_2 observed at 77 K with the NLDFT equilibrium isotherms for the unconnected cylindrical pores. All these results indicate that the pore size of controlled pore glass is actually greater than specified. The discrepancies in pore size dependences of the melting temperature of a confined solid and the hysteresis temperature of a gas−liquid phase transition between conventional mesoporous materials and mesoporous molecular sieves are ascribed to inaccuracy of a nominal pore size of the conventional mesoporous materials.

References and Notes

(1) Gregg, S. J.; Sing, K. S. W. *Adsorption, Surface Area, and Porosity*; Academic: New York, 1982; Chapter 3.
(2) Burgess, C. G. V.; Everett, D. H.; Nuttall, S. *Pure Appl. Chem.* **1989**, *61*, 1845.
(3) Ravikovitch, P. I.; Domhnail, S. C. O.; Neimark, A. V.; Schuth, F.; Unger, K. K. *Langmuir* **1995**, *11*, 4765.
(4) Morishige, K.; Shikimi, M. *J. Chem. Phys.* **1998**, *108*, 7821.
(5) Sonwane, C. G.; Bhatia, S. K. *Langmuir* **1999**, *15*, 5347.
(6) Machin, W. D. *Phys. Chem. Chem. Phys.* **2003**, *5*, 203.
(7) Gelb, L. D.; Gubbins, K. E.; Radhakrishnan, R.; Sliwinska-Bartkowiak, M. *Rep. Prog. Phys.* **1999**, *62*, 1573.
(8) Levitz, P.; Ehret, G.; Sinha, S. K.; Drake, J. M. *J. Chem. Phys.* **1991**, *95*, 6151.
(9) Kresge, C. T.; Leonowicz, M. E.; Roth, W. J.; Vartuli, J. C.; Beck, J. S. *Nature* (*London*) **1992**, *359*, 710.
(10) Zhao, D.; Huo, Q.; Feng, J.; Chmelka, B. F.; Stucky, G. D. *J. Am. Chem. Soc.* **1998**, *120*, 6024.
(11) Machin, W. D. *Langmuir* **1994**, *10*, 1235.
(12) Machin, W. D. *Langmuir* **1999**, *15*, 169.
(13) Morishige, K.; Fujii, H.; Uga, M.; Kinukawa, D. *Langmuir* **1997**, *13*, 3494.
(14) Morishige, K.; Ito, M. *J. Chem. Phys.* **2002**, *117*, 8036.
(15) Rennie, G. K.; Clifford, J. *J. Chem. Soc. Faraday Trans. 1* **1977**, *73*, 680.
(16) Morishige, K.; Kawano, K. *J. Chem. Phys.* **1999**, *110*, 4867.
(17) Schreiber, A.; Ketelsen, I.; Findenegg, G. H. *Phys. Chem. Chem. Phys.* **2001**, *3*, 1185.
(18) Pellenq, R. J.-M.; Rousseau, B.; Levitz, P. E. *Phys. Chem. Chem. Phys.* **2001**, *3*, 1207.
(19) Giauque, W. F.; Clayton, J. O. *J. Am. Chem. Soc.* **1933**, *55*, 4875.
(20) Streib, W. E.; Jordan, T. H.; Lipscomb, W. N. *J. Chem. Phys.* **1962**, *37*, 2962.
(21) Huber, P.; Wallacher, D.; Knorr, K. *J. Low Temp. Phys.* **1998**, *111*, 419.
(22) Huber, P.; Wallacher, D.; Knorr, K. *Phys. Rev. B* **1999**, *60*, 12666.
(23) Morishige, K.; Kawano, K. *J. Phys. Chem. B* **2000**, *104*, 2894.
(24) Kruk, M.; Jaroniec, M.; Ko, C. H.; Ryoo, R. *Chem. Mater.* **2000**, *12*, 1961.
(25) Neimark, A. V.; Ravikovitch, P. I. *Microporous Mesoporous Mater.* **2001**, *44*, 697.
(26) Younglove, B. A. *J. Phys. Chem. Ref. Data Suppl.* **1982**, *11*, 1.
(27) Morishige, K.; Inoue, K.; Imai, K. *Langmuir* **1996**, *12*, 4889.
(28) Sing, K. S. W.; Everett, D. H.; Haul, R. A. W.; Moscou, L.; Pierotti, R. A.; Rouquerol, J.; Siemieniewska, T. *Pure Appl. Chem.* **1985**, *57*, 603.
(29) Wong, A. P. Y.; Chan, M. H. W. *Phys. Rev. Lett.* **1990**, *65*, 2567.
(30) Litvan, G.; McIntosh, R. *Can. J. Chem.* **1963**, *41*, 3095.
(31) Huber, P.; Knorr, K. *Phys. Rev. B* **1999**, *60*, 12657.
(32) Duffy, J. A.; Alam, M. A. *Langmuir* **2000**, *16*, 9513.
(33) Morishige, K.; Kawano, K.; Hayashigi, T. *J. Phys. Chem. B* **2000**, *104*, 10298.
(34) Brown, D. W.; Sokol, P. E. Clarke, A. P.; Alam, M. A.; Nuttall, W. J. *J. Phys. Condens. Matter* **1997**, *9*, 7317.
(35) Wang, Y.; Snow, W. M.; Sokol, P. E. *J. Low Temp. Phys.* **1995**, *101*, 929.
(36) Charnaya, E. V.; Tien, C.; Lin, K. J.; Kumzerov, Yu. A. *Phys. Rev. B* **1998**, *58*, 11089.
(37) Wallacher, D.; Ackermann, R.; Huber, P.; Enderle, M.; Knorr, K. *Phys. Rev. B* **2001**, *64*, 184203.
(38) Coulomb, J. P.; Floquet, N.; Grillet, Y.; Llewellyn, P. L.; Kahn, R.; Andre, G. In *Mesoporous Molecular Sieves*; Unger, K. K., Kreysa, G., Baselt, J. P., Eds.; Studies in Surface Science and Catalysis, No. 128; Elsevier: Amsterdam, The Netherlands, 2000; p 235.
(39) Morishige, K.; Kawano, K. J. *Phys. Chem. B* **1999**, *103*, 7906.
(40) Morishige, K.; Kawano, K. *J. Chem. Phys.* **2000**, *112*, 11023.

(41) Hoinkis, E.; Rohl-Kuhn, B. In *Fundamentals of Adsorption*; Kaneko, K., Kanoh, H., Hanzawa, Y., Eds.; IK International: Tokyo, Japan, 2002; Vol. 7, p 601.
(42) Gelb, L. D.; Gubbins, K. E. *Langmuir* **1999**, *15*, 305.
(43) Gelb, L. D.; Gubbins, K. E. In *Fundamentals of Adsorption*; Kaneko, K., Kanoh, H., Hanzawa, Y., Eds.; IK International: Chiba, Japan, 2002; Vol. 7, p 333.
(44) Morishige, K.; Tateishi, N.; Fukuma, S. *J. Phys. Chem. B* **2003**, *107*, 5177.
(45) Barrett, E. P.; Joyner, L. G.; Halenda, P. P. *J. Am. Chem. Soc.* **1951**, *73*, 373.
(46) Morishige, K.; Nakamura, Y. *Langmuir*, in press.
(47) Qiao, Y.; Schoenhoff, M.; Findenegg, G. H. *Langmuir* **2003**, *19*, 6160.